Reproducing the present-day mantle structure using forward mantle convection models since the Cretaceous

Debanjan Pal*, Attreyee Ghosh
Centre for Earth Sciences, Indian Institute of Science, Bangalore, India *debanjanpal@iisc.ac.in
Abstract Number: DI13B-0034
AGU23 San Francisco, CA & Online Everywhere 11-15 December 2023

1. INTRODUCTION

In this study, we perform forward mantle convection modeling starting from 140 Ma to predict present-day mantle structure[1].
The main questions addressed in this study are:
1) Investigate how different slab structures came into being at major subduction zones.
2) What factors affect the location and generation of plumes ?
3) How do lateral viscosity variations (LVV) affect predicted mantle structure?
4) What role does a thin, weak layer below 660 km play?
5) Whether Large Low Shear Velocity Provinces (LLSVPs) are thermal or thermochemical in nature?
6) Effect of Clapeyron slope on slab stagnation at 660 km.
7) Find a suitable initial condition that simultaneously matches seismic tomography models (S40RTS[2] and TX2019S[3]) and the observed geoid.

2. METHODOLOGY

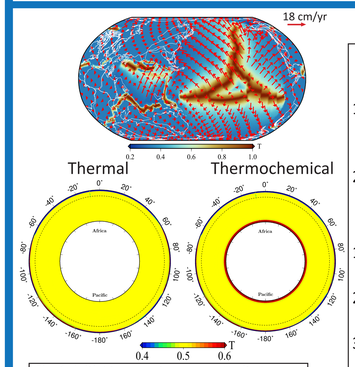

Fig. 1: Initial temperature and velocity boundary condition at 140 Ma (T denotes non-dimensionalized temperature).

Mantle convection solver: CitcomS

Density Structure

1) Temperature heterogeneity in the oceanic lithosphere derieved from sea floor age grid[4] at 140 Ma (Figure 1).
2) Imposed surface plate velocity from plate reconstruction[5] (Figure 1).

Viscosity Structure

1) The mantle is divided into 4 layers of different viscosities (Figure 2).
2) In addition we test the effect of a thin weak layer below the transition zone.
3) Lateral viscoisty variations in our models are temperature dependent.

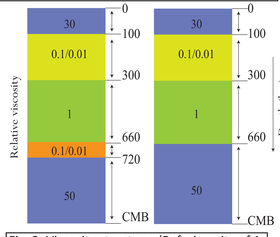

Fig. 2: Viscosity structure (Ref. viscosity of 1 corresponds to 10^{21} Pas).

Models shown here

Case 1: Reference thermal case
Case 6: Reference thermal case - LVV
Case 9: Reference thermochemical case (Thermochemical pile with buoyancy ratio, B=0.15)
Case 11: Denser thermochemical case (B=1.0)
Case 16: Reference thermochemical case (B=0.15) + Clayperon slope (660 km) (-6 MPa/K)

Seismic Filtering

For a meaningful comparison with tomography models, we perform seismic filtering on our geodynamic models using the S40RTS tomography filter[6,7].

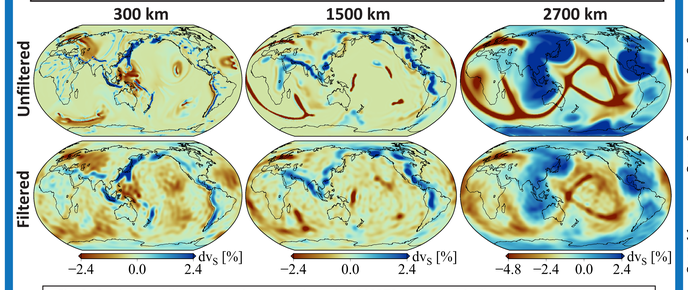

Fig. 3: Original and filtered velocity anomalies using S40RTS tomographic filter from one of the models.

3. PREDICTED MANTLE STRUCTURE

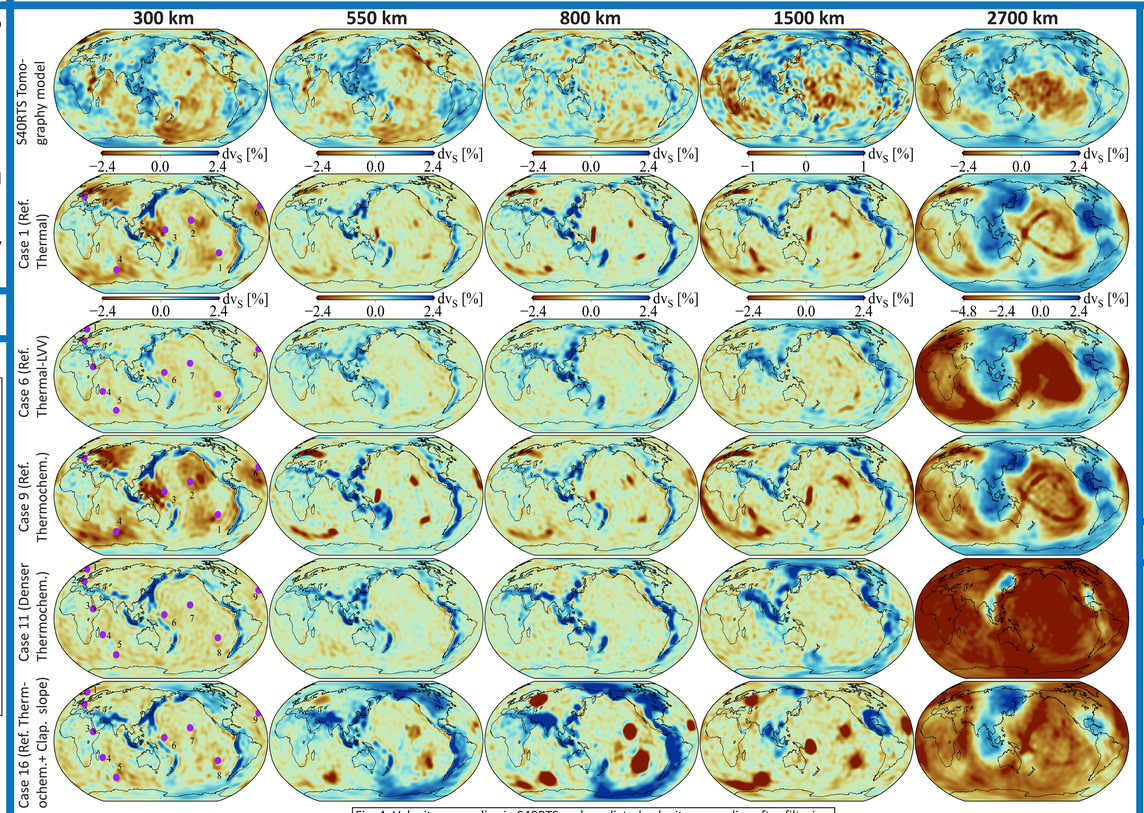

Fig. 4: Velocity anomalies in S40RTS and predicted velocity anomalies after filtering.

SLAB STRUCTURES ACROSS MAJOR SUBDUCTION ZONES

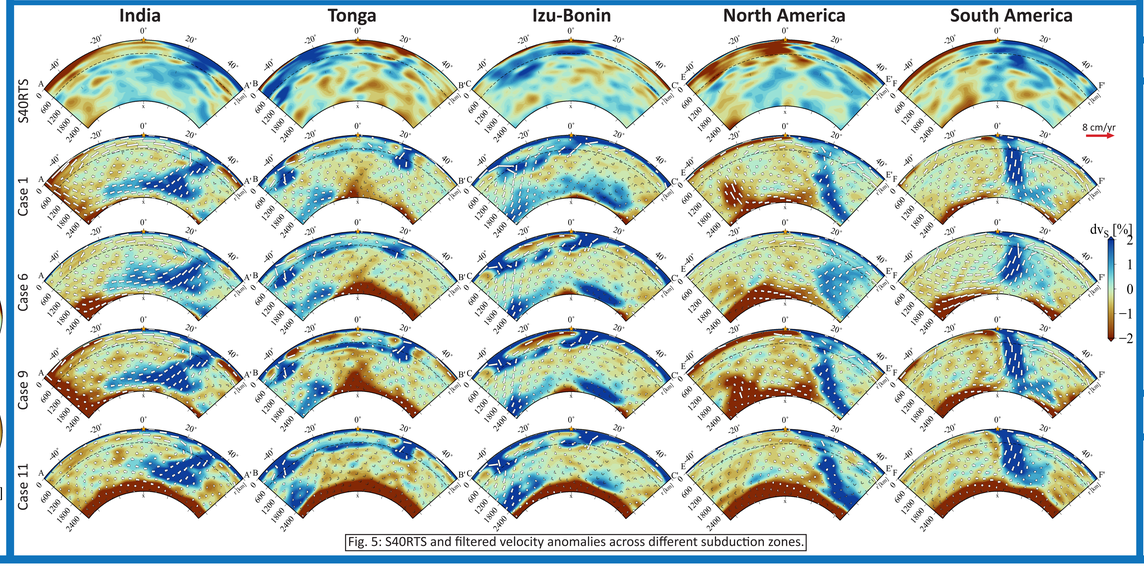

Fig. 5: S40RTS and filtered velocity anomalies across different subduction zones.

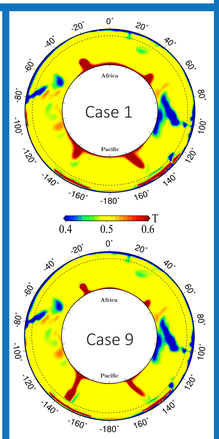

Fig. 6: Predicted present day mantle structure from reference thermal and thermochemical cases.

4. PREDICTED GEOID ANOMALY

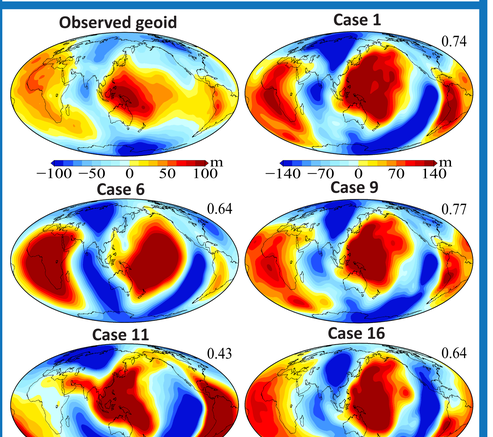

Fig. 7: Geoid anomalies. Numbers in the top right denote the correlation with the observed geoid[8].

5. AVERAGE CORRELATION

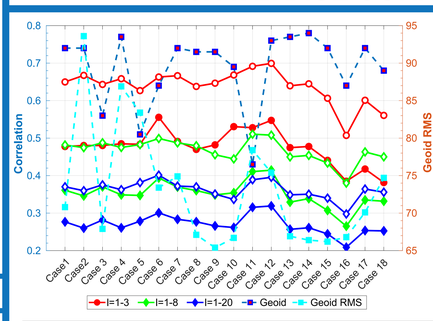

Models

Case 2: Ref. Thermal - global thin weak layer at 660
Case 3: Ref. Thermal + global thin weak layer at 660 with viscoity of 0.01 (0.1 in all other cases)
Case 4: Ref. Thermal + regional thin weak layer at 660
Case 5: Ref. Thermal - global thin weak layer at 660 + asthenosphere viscosity 0.01 (0.1 in all other cases)
Cases 7 and 8: Ref. Thermal + internal heat generation rates (H) 0 and 200 (H=100 for all other cases)
Case 10: Dense thermochemical pile (B=0.25)
Case 12: Ref. Thermochemical + viscous LLSVPs
Cases 13 and 14: Ref. Thermochemical + Clap. slope (-2.5 MPa/K, density jump of 5% and 8% across 660)
Case 15: Ref. Thermochemical + Clap. slope (-4 MPa/K)
Cases 17 and 18: Models start at 160 and 200 Ma, respectively.

Fig. 8: Open and solid symbols denote correlation with S40RTS and TX2019S.

6. CONCLUSIONS

1. Our models are able to predict slab structures that are consistent with the seismic tomography models.
2. The shape and location of the LLSVPs also match well with the tomography models.
3. The downwelling slabs perturb the LLSVPs and generate plumes along their edges. The plume locations are more or less well-matched with tomography models.
4. Increasing the density of the chemical piles makes the LLSVPs stable for a geological timescale. However, too heavy a chemical pile inhibits plume generation and also degrades the geoid fit.
5. Both thermal and thermochemical cases are able to match the mantle structure and the geoid quite well.
6. A very steep Clapyeron slope (-6 MPa/K) does not match the mantle structure and causes the slabs to stagnate in the transition zone and also degrades the geoid fit.
7. Although some models match the observed seismic structure well, they fail to match the observed geoid (Figure 8).

7. REFERENCES

1. Pal and Ghosh, Present day mantle structure from global mantle convection models since the Cretaceous, Under revision in GJI.
2. Ritsema et al., 2011. S40RTS: a degree-40 shear-velocity model for the mantle from new Rayleigh wave dispersion, teleseismic traveltime and normal-mode splitting function measurements. GJI, 184(3).
3. Lu et al., 2019. TX2019slab: A new P and S tomography model incorporating subducting slabs. JGR, 124(11).
4. Muller et al., 2016. Ocean basin evolution and global-scale plate reorganization events since Pangea breakup. Annu. Rev. Earth Planet. Sci., 44.
5. Zahirovic et al., 2015. Tectonic speed limits from plate kinematic reconstructions. EPSL, 418.
6. Koelemeijer et al., 2018. Constraints on the presence of post-perovskite in Earth's lowermost mantle from tomographic-geodynamic model comparisons. EPSL, 494.
7. Ritsema et al., 2007. Tomographic filtering of geodynamic models: Implications for model interpretation and large-scale mantle structure. JGR, 112(B1).
8. Nakiboglu, S. 2010. Hydrostatic theory of the Earth and its mechanical implications. Phys. Earth Planet. Inter., 28(4).